Research article

Journal of RAMAN SPECTROSCOPY

Received: 3 March 2014 Revised: 3 April 2014 Accepted: 5 May 2014 Published online in Wiley Online Library: 27 May 2014

(wileyonlinelibrary.com) DOI 10.1002/jrs.4506

The interface between nacre and bone after implantation in the sheep: a nanotomographic and Raman study

Florence Pascaretti-Grizon,[a] Hélène Libouban,[a] Georges Camprasse,[c] Serge Camprasse,[c] Romain Mallet[a,b] and Daniel Chappard[a,b]*

Orthopedic bone devices can be prepared from the shells of giant pearl oysters. Nacre is biocompatible and composed of calcium carbonate (aragonite). Direct welding of bone onto the biomaterial surface has been reported but poorly investigated. Nacre from *Pinctada maxima* was used to prepare plates, screws and rods. Five sheep were implanted in the first metatarsus under general anesthesia and killed 2 months later. Bones were harvested and fixed in formalin. Analysis was performed by nanotomography and histology after embedding in poly(methyl methacrylate). Polished sections were imaged by scanning electron microscopy then analyzed on a Raman microscope. Nanotomography and histology evidenced the newly apposed bone composed of thin trabeculae with a lower mineralization than mature bone. Erosion of the nacre was also easily observed. The bone/nacre interface presented a characteristic toothed-comb appearance. Raman spectroscopy identified the typical bands of aragonite (1091 and 711 cm^{-1}) in the devices. At a distance from the interface, the bone matrix presented the typical bands of hydroxyapatite at 960, 1044 and 594–610 cm^{-1} with the amide bands of collagen at 1250 cm^{-1}. At the bone/nacre interface, a phosphate-rich layer was observed without proteins. The newly formed bone units exhibited a band at 1075 cm^{-1} corresponding to a high amount of B-carbonate substitution. The carbonate/phosphate ratio decreased between new and mature bone, and crystallinity was improved. Raman spectroscopy confirmed the modifications of the bone matrix around the nacre implant and the direct apposition of bone without an interposing organic layer between the calcium carbonate (nacre) and the calcium phosphate (hydroxyapatite). Copyright © 2014 John Wiley & Sons, Ltd.

Keywords: nacre; bone; orthopedic device; nanotomography; Raman analysis

Introduction

Although the gold standard for bone substitutes remains autograft, there is sustained research worldwide to develop new substitutes that could be available in large quantities. These materials intend to reduce several shortcomings associated with harvesting autogenous bone such as the high incidence of substantial morbidity.[1,2] Synthetic bioceramics such as β-tricalcium phosphate or hydroxyapatite granules are biocompatible materials suitable for filling bone defects, but they are usually brittle with relatively low tensile properties and they cannot be used in weight-bearing areas. Plates or screws for orthopedic usage have been prepared from synthetic polymers such as polylactic or polyglycolic acid, either alone or associated with hydroxyapatite.[3]

The underlying idea is to obtain devices that are bioerodible in the surface and could be used as bone implants and will not necessitate a second surgical event for removal, the loads having been slowly transferred from the device to the remodeled bone during the healing phase. Among suitable bone substitutes, nacre has been proposed as a natural biocompatible and osteoconductive biomaterial.[4] Nacre can be easily obtained from the shell of several varieties of giant oysters such as *Pinctada maxima*. The material is composed of aragonite (a variety of calcium carbonate) and presents excellent compressive stress properties close from bone mechanical properties (Young's modulus is 30–40 GPa for nacre *vs* 20 GPa for bone, and resistance to failure is 185–200 MPa *vs* 140 MPa for bone).[5,6] Because of its layered architecture alternating between a mineral component and an organic component, the biomaterial presents a lamellar structure particularly adapted to the absorption and distribution of the forces and impacts opposing rupture. That hierarchical organization and other structural features play an important role in the remarkable mechanical performance (toughness, strength, etc). Biodegradation of nacre after bone implantation has been studied in *in vitro* studies [7] and after *in vivo* experiments.[8–10] Similarly, osteoblast stimulation has also been reported *in vitro* [11,12] and *in vivo*.[10] Because the material can be easily machined to produce screws or plates suitable for orthopedics, the good cytocompatibility of nacre could represent

* *Correspondence to: Daniel Chappard, GEROM – LHEA, IRIS-IBS Institut de Biologie en Santé, LUNAM Université Nantes Angers Le Mans, CHU d'Angers, 49933 Angers Cedex, France.*
E-mail: daniel.chappard@univ-angers.fr

a *GEROM Groupe Etudes Remodelage Osseux et bioMatériaux – LHEA, IRIS-IBS Institut de Biologie en Santé, CHU d'Angers, LUNAM Université, 49933 Angers Cedex, France*

b *SCIAM, Service Commun d'Imagerie et Analyses Microscopiques, IRIS-IBS Institut de Biologie en Santé, CHU d'Angers, LUNAM Université, 49933 Angers Cedex, France*

c *MEGA BIO PHARMA, 91560 Crosne, France*

an additional interest because no inflammation has been described after bone implantation, at the difference of devices made with polylactic and polyglycolic acid.[3,13] After implantation of pieces of nacre in bone defects, a direct welding of bone and nacre is observed.[14] Microradiographic studies have revealed that a typical toothed-comb microstructure interface was present at the frontier between bone and nacre.[8,15,16] However, the exact nature of this interface has been poorly explored. The aim of the present study was to analyze the bone–nacre interface to provide a better characterization of nacre biocompatibility. Large orthopedic devices (plates and screws) were implanted in the sheep, and the interface was studied by nanocomputerized tomography (nanoCT), scanning electron microscopy with microanalysis, histochemistry and Raman spectroscopy.

Material and methods

The nacre biomaterial

Orthopedic devices were prepared from the inner shell of the giant oyster *P. maxima* coming from an oyster park in Indonesia. Oysters were approximately 20 cm in diameter corresponding to a mean age of 7–12 years old. Screws, rods and plates were obtained through a process, in which patent applications are pending. It combines a series of physicochemical treatments, cutting and coating operations providing, from the compact raw nacre, appropriate nonremovable devices suitable for long-term osteosynthesis and made of this hybrid semisynthetic material. Devices were sterilized by γ radiation at 25 Gy and stored in a double plastic bag until use.

Animal implantation: surgical procedure

Five sheep from the Romane strain INRA 401 were obtained from a French sheep breeding center in Bourges (France). Animals (~8 months old) were transferred to Centre de Recherche d'Alfort BioMédicale (Biomedical Research Centre) in École nationale vétérinaire d'Alfort (National Veterinary School of Alfort) and acclimated for 5 days to local conditions. The experiment was conducted with ethical principles for animal studies and good clinical standards after having received the agreement of the veterinary ethical committee (Cometh/ENVA/UPEC #12-013; 10/04//12-1). Before surgery, animals were premedicated by sodium thiopenthal. General anesthesia was induced with an intravenous perfusion of ketamine (1 mg/kg) and after an endotracheal intubation maintained with isoflurane provided by an anesthetic apparatus. Cardiac monitoring, pulse and inspired gases (CO_2 and halogenated) were recorded throughout the operating time. The first metatarsus was exposed using a standard lateral approach. Cylindrical holes adapted to the nacre devices were created with an electric rotary instrument used for dental surgery. Drilling was performed at low speed and under irrigation with physiologic saline to avoid heating. Nacre devices were placed in the drill holes, and the incision was closed with resorbable sutures. Benzyl penicillin–dihydrostreptomycin was given by intramuscular injection as a prophylactic antibiotic. Pain was avoided by morphine injection (0.1 mg kg^{-1}) every 2 h during surgery and at 20 mg SC during 5 days postsurgery.

Sheep were killed after 2 months with an intravenous injection of natrium pentobarbital iv. Bones were defleshed, harvested and fixed in formalin before shipping to the bone laboratory.

Histological techniques

Bones were radiographed on a numeric system (Faxitron, Edimex, Angers) in order to determine the precise location of the nacre implants. Then, bones were transferred while in the fixative in a nanocomputed tomograph (Nanotom, Phoenix, GE, USA). NanoCT analysis was performed at 100 kV and 150 μA. Five projection images were averaged every 750 ms, and the rotation angle was 0.2° with a pixel size of 10.03 μm. Image reconstruction was performed on the projection images with the DATOS software (Phoenix, GE), and a stack of 2D sections was obtained for each specimen. The image resolution was between 0.6 and 0.8 μm $pixel^{-1}$. 3D models were obtained with VG StudioMax (Volume Graphics GmbH, Heidelberg, Germany). On the 3D models, reslicing is possible to expose the different areas of interest.

Bone samples were then dehydrated and embedded undecalcified in poly(methyl methacrylate) (pMMA) as previously reported. Blocks were then sectioned with a diamond saw (Accutom, Struers, France) in 500 μm thick slices. For screws, the slice passing through the central zone was selected. Slices were polished on an automatic polishing machine (Struers) to a 1 μm finish with diamond particles. Then, slices received one of the following treatments: (1) Histological analysis was performed after acid etching of the surface with 0.1% formic acid in distilled water for 4 min followed by staining with borax–toluidine blue during 45 min. Slices were dried and analyzed on an Olympus BX 51 microscope. The bone/nacre interface was determined (expressed in %), (2) scanning electron microscopy (SEM) was performed (after carbon coating of the slices) with an EVO LS10 microscope (Carl Zeiss Ltd, Nanterre, France) equipped with a five quadrant semiconductor backscattered electron (BSE) detector, (3) after SEM analysis, slices were rapidly polished with diamond particles to remove the carbon coating. They were then analyzed on a Senterra Raman microscope with the OPUS 5.5 software (Bruker Optics, Ettlingen, Germany). The excitation laser wavelengths were at 532 and 785 nm with an excitation power of 50 mw and 8.12-cm^{-1} resolution for nacre. Because bone has a strong autofluorescence of the matrix with the 532-nm laser, the analysis of the bone/nacre interface was conducted with the 785-nm laser. The final spectra were obtained by averaging five scans of 20 s in each case. Spectra were obtained on the areas previously identified by SEM and imaged with the video epi-illumination of the Senterra microscope. An automatic baseline was applied, and all spectra were normalized on the 819-cm^{-1} peak of pMMA. Raman analysis of the raw nacre material was also obtained from a dry shell of a *P. maxima* oyster. In the case of bone tissues, it is possible to determine the degree of mineralization (or mineral to organic matrix ratio) of the matrix as the ratio of the 960-cm^{-1} phosphate band by the 1590–1720-cm^{-1} amide 1 band. Mineral crystallinity was obtained by determining the band width at half the peak intensity of the 960-cm^{-1} phosphate band and expressed as 1 $bandwidth^{-1}$.[17] The carbonate to phosphate ratio was obtained by dividing the intensity of the 1075-cm^{-1} CO_3 band by the 960-cm^{-1} phosphate band.[18,19]

Results

Animals and histology

No animal developed infection or side effects after implantation. Figure 1 illustrates the *postmortem* radiographic and histological

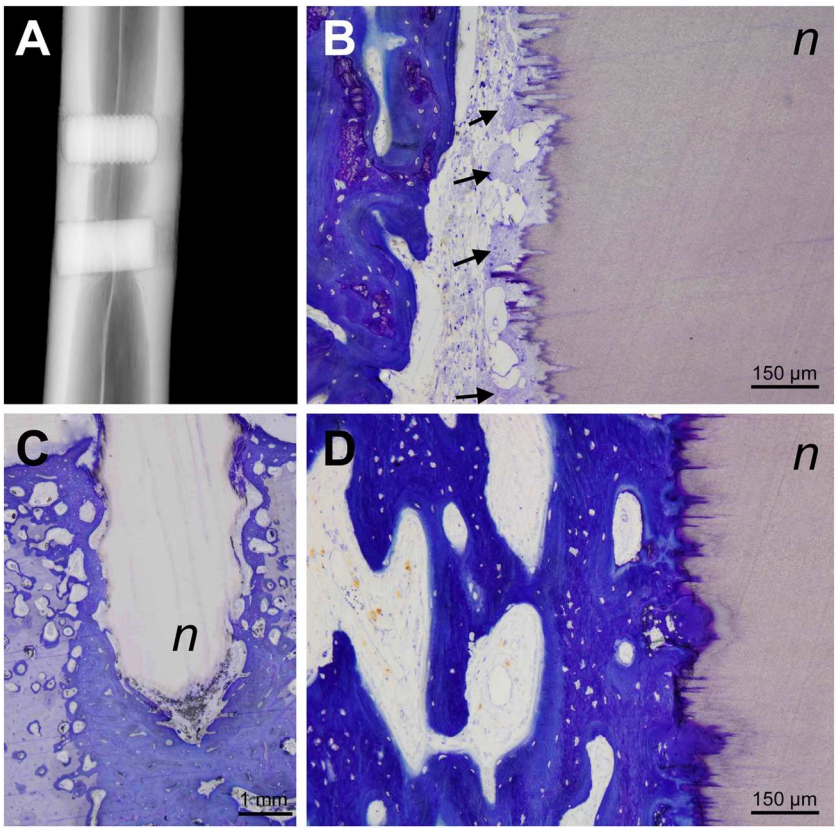

Figure 1. (A) Radiological aspect of a screw and a plate prepared from *P. maxima* nacre after a 2-month implantation period in the sheep. (B) Histological aspect of the nacre erosion by giant cells (arrows), (C) histological aspect of the screw appearing in panel A and exhibiting bone apposition and erosion of the material and (D) histological aspect at high magnification of the bone apposition onto nacre. Note the typical toothed-comb shape of the interface. Toluidine blue staining: Bone is in blue; nacre (n) is unstained.

aspects of the implantation of a screw and a plate. The nacre biomaterial was submitted to a simultaneous remodeling process that implied both erosion by giant macrophagic cells (Fig. 1B) and bone apposition on the previously eroded areas. Toluidine blue evidenced the presence of blue bony material interpenetrated in the surface irregularities of the nacre. The frontier between nacre and bone was slightly metachromatic and periodic acid–Schiff positive (data not shown). As classically reported with toluidine blue, the youngest bone structure units were more heavily stained than the oldest ones. Figure 1C illustrates a nacre screw at low magnification and evidences the net bone apposition around the screw and the partial erosion of the threads. A direct apposition of bone onto the nacre was evidenced and presented the characteristic toothed-comb aspect illustrated on Fig. 1D.

Nanotomographic study

Nanotomography allowed a 2D and 3D analysis of the interface between bone and the nacre implants. The typical aspect of bone apposition and biomaterial resorption appears on Fig. 2. Bone trabeculae were in direct contact with nacre, and the trabecular network was composed of thin trabeculae having a plexiform and highly connected disposition characteristic of woven bone. Eroded surfaces were clearly identified at the surface of the threads of the screw that appeared irregular. A direct bonding of bone at the biomaterial surface was evidenced on the different types of nacre devices.

Scanning electron microscopy

A typical image in the BSE mode of the interface between bone and nacre appears on Fig. 3A. In the BSE mode, the grey level parallels the amount of calcium present in the structure. Nacre containing high amounts of $CaCO_3$ appeared uniformly white. The margin of the implant that has been eroded by the giant cells had the characteristic toothed-comb shape previously identified on light microscopic sections. The bone matrix was more heterogeneous, and the different bone structure units had various grey levels depending on their constitution age: The youngest were less mineralized and appeared dark grey; the oldest were fully mineralized and were whiter.

Raman analysis

The spectra of raw and machined nacre appear on Fig. 4. The spectra exhibited the characteristic bands of orthorhombic aragonite. The spectrum of the machined aragonite was recorded using the two lasers. Machining of the material had no influence on the position of the bands, but the most noticeable difference between the two wavelengths was observed between 100 and 400 cm^{-1}. The $\nu 1$ peak of aragonite (symmetric stretching) was found at 1087 and 1091 cm^{-1} (respectively with the 532 and 785-nm laser), the $\nu 4$ peak at, respectively, 703 and 711 cm^{-1}. In the low wavenumber domain, the characteristic peaks were found at 154 and 207 cm^{-1} with the 532-nm laser, 153 and 282 cm^{-1} with the 785-nm laser. A typical area of analysis of

Journal of RAMAN SPECTROSCOPY

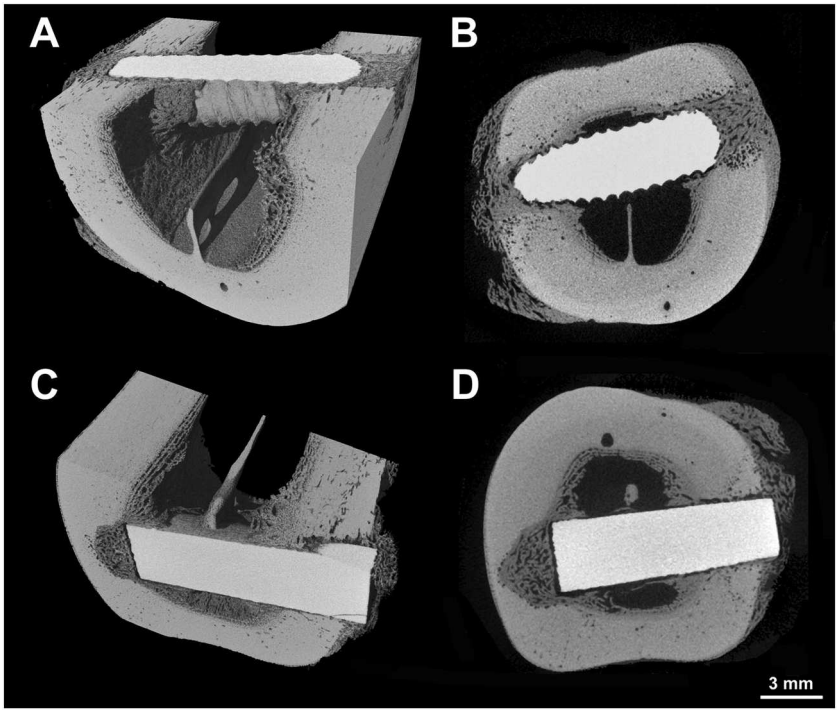

Figure 2. Nanotomographic analysis of an orthopedic screw and rod machined from *P. maxima* nacre. (A) 3D model of a screw implanted in a sheep metatarsus. Note the amount of newly formed bone at the surface of the implant both in the drilled hole but also extending from the inner endosteal surface. The threads are not regular, a sign of erosion by giant cells. (B) 2D section showing the intimate contact between bone and the nacre implant. Note the different mineralization degree between the newly formed bone and the mature one from the matrix. (C) 3D model of a nacre rod placed in a bone defect. The apposition of new bone is evidenced together with the rough surface of the implant as a result of erosion; (D) 2D section of the same rod, showing bone apposition, osteoconduction on the rod surface and signs of erosion.

the bone/nacre interface appears in Fig. 3B that is an enlargement of Fig. 3A viewed at a higher magnification under the videosystem of the Raman microscope. For convenience, Fig. 3C illustrates a similar region on a toluidine blue section viewed under the light microscope. Numbers identify the different spectra appearing on Fig. 5; all of them have been normalized on the 819-cm^{-1} band of the pMMA embedding medium. Position 1 was recorded at a high distance from the bone/nacre interface in a fully matured bone area. The characteristic peaks of the calcium-phosphate deposits (hydroxyapatite) are figured: $\nu1$ at 960 cm^{-1}, $\nu3$ at 1044 cm^{-1} and $\nu4$ at 594–610 cm^{-1}. The other peaks correspond to the collagen of the bony matrix with peaks at 1250 cm^{-1} (amide 3). The 1450-cm^{-1} peak represents the $-CH_2$ bending of proteins and pMMA; the 819-cm^{-1} peak corresponds to the symmetric CC4 from pMMA. The 1075-cm^{-1} band is attributed to the carbonate substitution of the –OH groups of hydroxyapatite. Spectrum 2 is obtained from immature bone that is mineralized (the presence of the 960, 594–610 and 1044-cm^{-1} peaks), but the $\nu3$ carbonate peak at 1075 cm^{-1} is higher. Spectrum 3 is obtained in the intermediary area that is heavily stained by toluidine blue on histological sections. It evidences the presence of phosphate at 960 and 594 cm^{-1} and pMMA, but no collagen is clearly observed. Spectrum 4 was recorded on the toothed-comb area and has a mixed composition: the typical bands of nacre at 1090 and 711 cm^{-1}; a small peak at 594 cm^{-1} identified some phosphate and pMMA at 1450 cm^{-1}. Spectrum 5 corresponded to nacre; no phosphate pMMA or amide peak was identified. The peak ratios are reported on Table 1 only for the first areas of interest because the amide 1 was too low in area 4 and absent in area 5.

Discussion

Bone is a composite material with an organic matrix mainly composed of type I collagen. The nature of the bone matrix, at the nanoscale, is also made of hydroxyapatite crystals (a calcium phosphate salt $Ca_5(PO_4)_3OH$) laid around the collagen fibers. Other levels of organization of the bone matrix exist with the arrangement into lamellae or woven bone (the texture level). The structure level consists in the disposition of the matrix in bone structure units (Haversian systems). Microarchitecture (organization into trabeculae) and macroarchitecture are the other highest level of organization.[20,21] Bone matrix is elaborated by osteoblasts as nonmineralized bone (osteoid tissue) that is then mineralized after a ~15-day maturation time.

Nacre is the internal part of the shell of pearl oysters. It has also a matrix with both an organic phase (made of polysaccharide β-chitin, lipids and acid proteins) that encapsulates polygonal crystals of aragonite (a $CaCO_3$ salt). However, the amount of the organic phase is very limited explaining that only transmission electron microscopy (TEM) or atomic force microscopy can show it in the form of ~20 nm thick layers.[22] In the present study, Raman analysis could not detect this organic phase within nacre; the only observable peaks were represented by the $\nu1$ and $\nu4$ carbonate bands.[23] Because the industrial process acts only on the organic phase of the nacre, it is likely that no difference could be evidenced between the raw and processed nacre. Bone apposition onto nacre has been studied in several papers. All of them report a direct apposition of the bone matrix onto the nacre implant: microradiography [8,9] or histology.[10,14,24,25] It is always reported that previous erosion by multinucleated giant cells occurs before bone is apposed.[9,25]

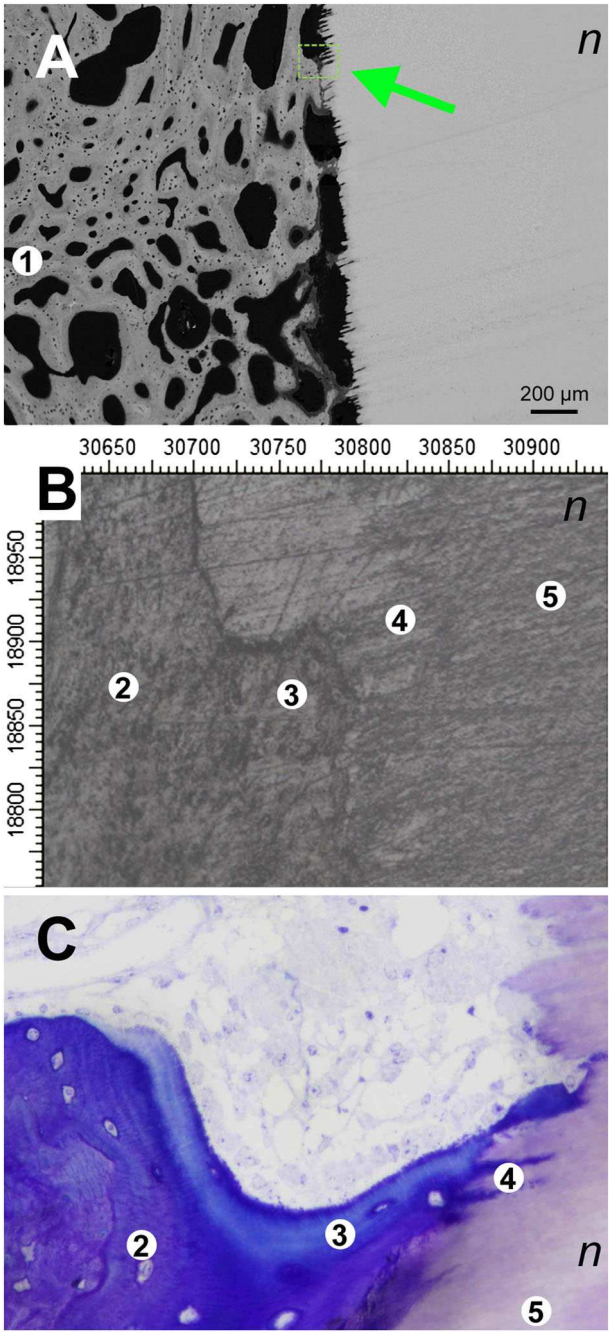

Figure 3. (A) Scanning electron microscopy with the backscattered electron mode of the interface between the nacre and bone. Note the irregular surface of the nacre implant (n) and the various degrees of mineralization of the bone structure units. An area analyzed by Raman spectroscopy is figured (green arrow and frame); (B) video image of the area highlighted in panel A and viewed under the Raman microscope. The numbers that illustrate the different locations were the spectra that were obtained. (C) A very similar region observed in light microscopy to illustrate the same locations.

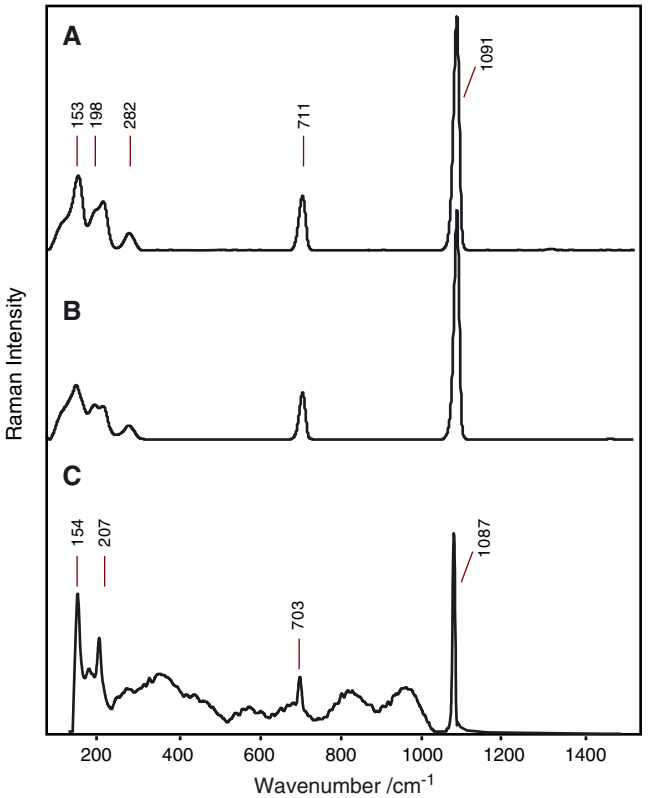

Figure 4. (A) Raman spectra of the nacre from *P. maxima* determined directly on the inner shell of the oyster with the 785-nm laser. (B) Spectrum of a machined nacre device obtained with the same laser. The characteristics peaks are figured. (C) Raman spectrum of the same nacre device obtained with the 532-nm laser.

So, the interface between bone and nacre is never linear but shows interdigitations (or toothed-comb aspect) that are because of the incorporation of the organic phase of nacre within the newly apposed bone.[8,9,25] TEM studies have revealed that there is no interposition of electron dense material between nacre and bone, but energy dispersive X-ray analysis has shown that a phosphate-rich layer is present.[25] Similar findings have also been reported with the implantation of coral exoskeletons made of $CaCO_3$.[26]

In the present study, nanotomography evidenced the direct apposition of woven bone onto the surface of nacre implants but also showed net signs of erosion at the surface of the machined devices. The technique provides more information than previous microradiographic studies because 3D study and mineralization degree of the newly formed bone can be evaluated. Raman analysis of the bone/nacre interface confirmed the absence of organic layer between the two tissues. The occurrence of the phosphate layer is evidenced at locations 3 and 4 with no apposition of collagen; the peak observed at 1450 cm^{-1} probably reflects the pMMA embedding medium (also associated with the 819-cm^{-1} peak). The presence of a large carbonate peak at 1075 cm^{-1} in the immature bone (location 2) is interesting because it reflects the carbonate substitution of hydroxyapatite and not the presence of nacre remnants. Bone mineralization is triggered by acidic proteins such as bone sialoprotein and propagated via the ectoenzyme alkaline phosphatase liberated by osteoblasts.[27,28] Mineralization of the structure units occurs in two steps. Primary mineralization begins ~15 days after the deposition of osteoid tissue (maturation lag-time) and processes until the matrix is loaded with ~70% of its capacity of hydroxyapatite within 120 days.[29] Secondary mineralization occurs more slowly over months to years.[30] After this period, osteoblasts have stopped their activity, but mineralization continues during months or years. This explains why the bone matrix appears heterogeneously mineralized with X-ray techniques such as microradiography or scanning electron

Journal of RAMAN SPECTROSCOPY

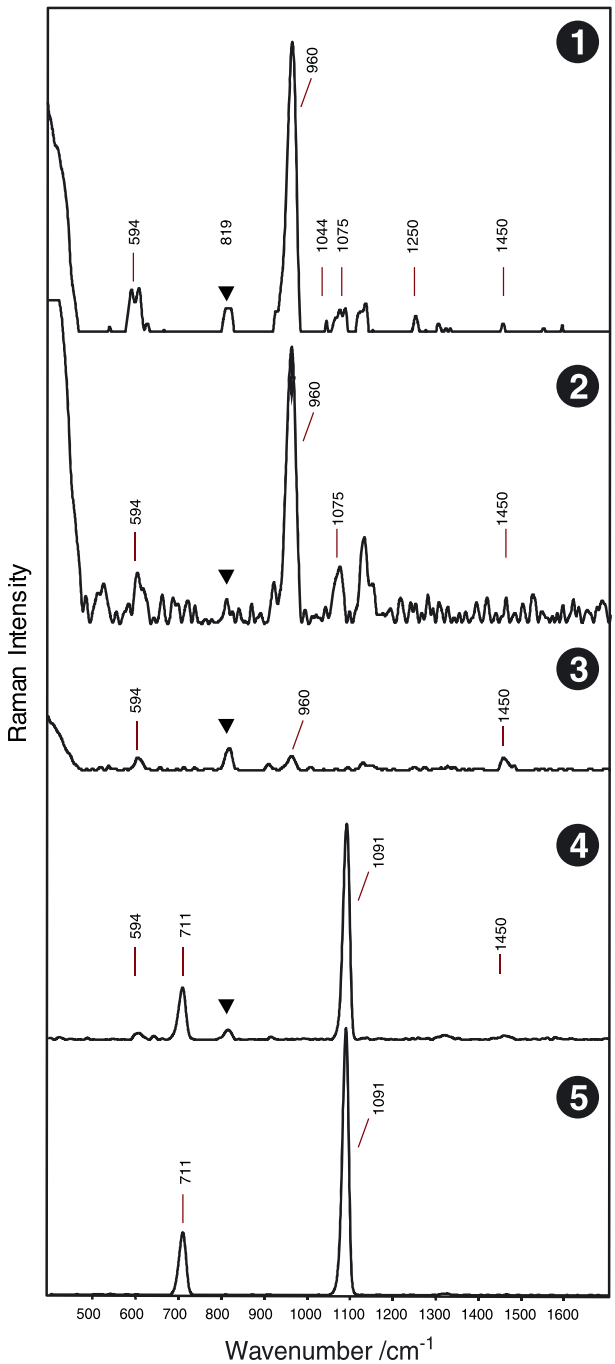

Figure 5. Raman spectra obtained in the different locations reported on Fig. 3. ① Typical aspect of the mature bone matrix exhibiting the characteristic bands of phosphates, amides and carbonate substitution at 1075 cm^{-1}. ② Immature bone showing a well-defined peak indicated a marked carbonate substitution of hydroxyapatite. ③ The bone–nacre interface showing the presence of phosphate.④ The nacre fringes showing the characteristic ν1 and ν4 peaks of aragonite at 1091 and 711 cm^{-1} together with phosphates at 594 cm^{-1}. ⑤ The spectrum of pure nacre is observed. All spectra have been normalized on the 819-cm^{-1} band of pMMA that has reduced the amount of other peaks, particularly the amide 1. The 819-cm^{-1} peak of pMMA is indicated by a black arrowhead on spectra 1 to 4; pure nacre does not contain pMMA.

microscopy in the BSE mode.[31] During this phase, an increase in the size of hydroxyapatite crystals and changes to their composition and structure are noted. The degree of mineralization increases, producing stiffer bone structure units. It was evidenced on parameters derived from Raman spectra by an increase in the degree of mineralization between locations 2 and 1. This is also clearly visible in a nanotomographic section and in BSE images where the younger structure units (and the woven bone) are less mineralized. At the same time, the hydroxyapatite crystal matures and the carbonate substitution regularly decreases.[32,33] In this study, the highest CO_3/PO_4 ratio was observed at the nacre–bone interface and then decreased in the newly formed bone structure units, and the value was low in mature bone (location 1). Simultaneously, crystallinity (or crystal maturity) that reflects chemical composition and purity was improved. In Raman spectroscopy, the crystallinity parameter decreases when hydroxyapatite crystals are less substituted (the 960-cm^{-1} peak appears more narrow).[18,19,34] This was also observed in this study, showing that the bony matrix gradually became more mature (Table 1).

Table 1. Mineralization parameters derived from peak analysis

	Location	Degree of mineralization	Crystallinity	CO_3/PO_4 ratio
Mature bone	1	32.04	0.11	0.077
Immature bone	2	13.57	0.16	0.109
Bone/Nacre interface	3	7.82	0.40	0.221

Conclusion

Nacre is a biomaterial suitable for bone repair. Devices having suitable mechanical properties for orthopedic use can be prepared in the form of screws, rods or plates.[9,15,16] Nacre is eroded in the surface by giant cells that create an irregular toothed-comb surface on which osteoblasts can appose bone directly without a layer of organic or fibrous material. A phosphate layer is first apposed onto nacre before newly formed bone structure units are laid down. The quality of the bony matrix progressively increases, and Raman microspectroscopy evidenced a reduction in carbonate substitution with maturation of hydroxyapatite crystals.

Acknowledgements

This work was made possible by grants from Contrat Region Pays de la Loire: Bioregos2 program. Many thanks are given to Mrs Lechat for secretarial assistance.

Conflict of interest

Georges and Serge Camprasse are scientific cooperators at MEGA BIO PHARMA. However, they took an active place in this study and performed the surgical implantations.

References

[1] E. D. Arrington, W. J. Smith, H. G. Chambers, A. L. Bucknell, N. A. Davino, *Clin. Orthop.* **1996**, *329*, 300.
[2] J. A. Goulet, L. E. Senunas, G. L. DeSilva, M. L. V. Greenfield, *Clin. Orthop.* **1997**, *339*, 76.
[3] S. Park, J. H. Kim, I. H. Kim, M. Lee, S. Heo, H. Kim, E. H. Kim, Y. B. Choy, C. Y. Heo, *J. Craniofac. Surg.* **2013**, *24*, 1021.
[4] L. P. Mouries, M. J. Almeida, C. Milet, S. Berland, E. Lopez, *Comp. Biochem. Physiol. B Biochem. Mol. Biol.* **2002**, *132*, 217.

[5] J. M. Cognet, J. C. Fricain, A. F. Réau, B. Lavignolle, C. Baquey, Y. Lepeticorps, *Rev. Chir. Orthop. Répar. App. Mot.* **2003**, *89*, 346.
[6] S. Hamza, N. Slimane, Z. Azari, G. Pluvinage, *Appl. Surf. Sci.* **2012**, *246*, 485.
[7] D. Duplat, A. Chabadel, M. Gallet, S. Berland, L. Bédouet, M. Rousseau, S. Kamel, C. Milet, P. Jurdic, M. Brazier, *Biomaterials* **2007**, *28*, 2155.
[8] S. Berland, O. Delattre, S. Borzeix, Y. Catonne, E. Lopez, *Biomaterials* **2005**, *26*, 2767.
[9] O. Delattre, Y. Catonne, S. Berland, S. Borzeix, E. Lopez, *Eur. J. Orthop. Surg. Traumatol.* **1997**, *7*, 143.
[10] M. Lamghari, S. Berland, A. Laurent, H. Huet, E. Lopez, *Biomaterials* **2001**, *22*, 555.
[11] E. Lopez, B. Vidal, S. Berland, S. Camprasse, G. Camprasse, C. Silve, *Tissue Cell* **1992**, *24*, 667.
[12] C. Silve, E. Lopez, B. Vidal, D. C. Smith, S. Camprasse, G. Camprasse, G. Couly, *Calcif. Tissue Int.* **1992**, *51*, 363.
[13] S. J. Yoon, S. H. Kim, H. J. Ha, Y. K. Ko, J. W. So, M. S. Kim, Y. I. Yang, G. Khang, J. M. Rhee, H. B. Lee, *Tissue Eng. Part A* **2008**, *14*, 539.
[14] C. Milet, S. Berland, M. Lamghari, L. Mouries, C. Jolly, S. Borzeix, D. Doumenc, E. Lopez, *Comptes Rendus Palevol* **2004**, *3*, 493.
[15] S. Camprasse, G. Camprasse, M. Pouzol, E. Lopez, *Clin. Mater.* **1990**, *5*, 235.
[16] E. Lopez, B. Vidal, S. Berland, C. Bozon, G. Camprasse, S. Camprasse, *Implantodontie* **1991**, *3*, 13.
[17] J. J. Freeman, B. Wopenka, M. J. Silva, J. D. Pasteris, *Calcif. Tissue Int.* **2001**, *68*, 156.
[18] O. Akkus, F. Adar, M. B. Schaffler, *Bone* **2004**, *34*, 443.
[19] O. Akkus, A. Polyakova-Akkus, F. Adar, M. B. Schaffler, *J. Bone Miner. Res.* **2003**, *18*, 1012.
[20] D. Chappard, M. F. Baslé, E. Legrand, M. Audran, *Morphologie* **2008**, *92*, 162.
[21] D. Chappard, M. F. Baslé, E. Legrand, M. Audran, *Osteoporos. Int.* **2011**, *22*, 2225.
[22] M. Rousseau, E. Lopez, P. Stempfle, M. Brendle, L. Franke, A. Guette, R. Naslain, X. Bourrat, *Biomaterials* **2005**, *26*, 6254.
[23] L. Xiang, J. Su, G. Zheng, J. Liang, G. Zhang, H. Wang, L. Xie, R. Zhang, *PlosOne* **2013**, *8*, e66564.
[24] M. Lamghari, M. J. Almeida, S. Berland, H. Huet, A. Laurent, C. Milet, E. Lopez, *Bone* **1999**, *25*, 91S.
[25] H. Liao, H. Mutvei, M. Sjostrom, L. Hammarstrom, J. Li, *Biomaterials* **2000**, *21*, 457.
[26] C. Müller-Mai, C. Voigt, S. de Almeida Reis, H. Herbst, U. Gross, *J. Mater. Sci.-Mater. Med.* **1996**, *7*, 479.
[27] G. K. Hunter, H. A. Goldberg, *Biochem. J.* **1994**, *302*(Pt 1), 175.
[28] M. P. Whyte, M. Landt, L. M. Ryan, R. A. Mulivor, P. S. Henthorn, K. N. Fedde, J. D. Mahuren, S. P. Coburn, *J. Clin. Invest.* **1995**, *95*, 1440.
[29] B. M. Misof, P. Roschger, F. Cosman, E. S. Kurland, W. Tesch, P. Messmer, D. W. Dempster, J. Nieves, E. Shane, P. Fratzl, K. Klaushofer, J. Bilezikian, R. Lindsay, *J. Clin. Endocrinol. Metab.* **2003**, *88*, 1150.
[30] G. Boivin, P. J. Meunier, *Osteoporos. Int.* **2003**, *14*(Suppl 3), S19.
[31] P. Roschger, P. Fratzl, J. Eschberger, K. Klaushofer, *Bone* **1998**, *23*, 319.
[32] P. Fratzl, H. Gupta, E. Paschalis, P. Roschger, *J. Mater. Chem.* **2004**, *14*, 2115.
[33] E. P. Paschalis, F. Betts, E. DiCarlo, R. Mendelsohn, A. L. Boskey, *Calcif. Tissue Int.* **1997**, *61*, 480.
[34] S. Bohic, C. Rey, A. Legrand, H. Sfihi, R. Rohanizadeh, C. Martel, A. Barbier, G. Daculsi, *Bone* **2000**, *26*, 341.